Robust Control Based on H_∞ and Linear Quadratic Gaussian of Load Frequency Control of Power Systems Integrated with Wind Energy System

Ali M. Eltamaly, Ahmed A. Zaki Diab, and Ahmed G. Abo-Khalil

Abstract This chapter introduces a robust control scheme of load frequency control (LFC) of a micro-grid system integrated with a wind energy system. The control scheme is based on H_∞ and linear quadratic Gaussian techniques. The main idea of the control design is to be stable against the parameter's uncertainties and the load disturbance. A complete model of the power system with the DFIG has been linearized. This model has been utilized to design both controllers of H_∞ and linear quadratic Gaussian. The H_∞ is designed by optimal selecting of the weighting functions to ensure the robustness and to enhance the overall performance. Also, the full states considering the frequency deviation are assessed based on the standard Kalman filter method. Moreover, the states of the system are applied with the linear quadratic Gaussian feedback optimal control performance under normal and abnormal operating conditions. Simulation tests are applied with the purpose of validation of the overall controllers' performance. The results proved the superiority of the planned integration of the wind energy system with the micro-grid.

Keywords Robust control · Load frequency control · Linear quadratic gaussian · H_∞ · Wind energy system

A. M. Eltamaly (✉)
Sustainable Energy Technologies Center, King Saud University, Riyadh 11421, Saudi Arabia
e-mail: eltamaly@ksu.edu.sa

Electrical Engineering Department, Mansoura University, Mansoura, Egypt

K.A. CARE Energy Research and Innovation Center, Riyadh 11421, Saudi Arabia

A. A. Zaki Diab
Electrical Engineering Department, Minia University, Minia, Egypt
e-mail: a.diab@mu.edu.eg

A. G. Abo-Khalil
Department of Electrical Engineering, College of Engineering, Majmaah University, Almajmaah 11952, Saudi Arabia
e-mail: a.abokhalil@mu.edu.sa

Department of Electrical Engineering, College of Engineering, Assuit University, Assuit 71515, Egypt

A. M. Eltamaly et al. (eds.), *Control and Operation of Grid-Connected Wind Energy Systems*, Green Energy and Technology,
https://doi.org/10.1007/978-3-030-64336-2_4

1 Introduction

In recent years, wind energy systems have been used to feed loads in remote and central areas. The wind energy applications are showing great interest due to their clean and sustainable nature. The advanced control system remedies the effects of the intermittent nature of the wind energy and it can be used widely even with weak power systems. This chapter is introduced to present a novel control system that enhances the stability of wind energy systems in case of normal and abnormal operation in micro-grids. In recent years, many control approaches are introduced to act with the impacts of load disturbance to regulate the frequency and voltages to the normal operating ranges. The variation in the frequency of the power system mainly depends on active power. Also, voltage control is affected by the variation of the reactive power too [1–4]. Therefore, the control problem of the power system is decoupled into two independent issues. The first one is the load frequency control (LFC), which is affected substantially by the active power control. The other one is to control the voltage based on regulating the reactive power. LFC is the main point of research in this chapter.

Energy and environmental topics are directed to integrating more renewable energies into power systems. Wind energy systems are rapidly increasing and its worldwide production is forecasted to produce to around 2000 GW in 2030 and 5000 GW in 2050 [5]. Hence, the integrations of the Wind Energy System (WES) with the power systems are very interesting topics for researchers. Many wind turbines (WTs) have been developed, among these WTs, the variable-speed wind turbines (VSWTs) have been considered as the best option for wind energy systems [6–12]. The inertial performance of WTs has been reported in Refs. [6, 10]. A comparison among the fixed-speed wind turbines (FSWTs) and doubly fed induction generator (DFIG) based WTs has been presented in [6]. Moreover, the simulation results had shown that FSWTs and DFIG-based WTs affect the frequency response of small power systems or micro-grids [6]. In Ref. [10], the presented results showed that an additional loop should be applied to enhance the machine inertial response of the WTs.

In recent years, many control schemes are applied to enhance the overall performance of such systems [12–14]. In Refs. [3, 15, 16], researchers applied the robust adaptive methods to act with the uncertainties of the parameters. Other researchers applied the Fuzzy logic controllers LFC in a two-area power system [17]. Others applied the artificial intelligence (AI) and genetic algorithms (GA) based controllers to LFC in [18, 19]. In Ref. [20], the H_∞ controller is applied and verified to control the photovoltaic pumping system. In Ref. [4], a robust control system concerning the linear quadratic Gaussian (LQG) and coefficient diagram method has been designed to LFC of a three-area power system. Also, adaptive model predictive control (AMPC) has been applied for solving the control issue of the LFC in the presence of a wind energy system [9]. For this reason, in this Chapter, the LFC for a single-area power system integrated with WES is considered using the combination of H_∞ and LQG controllers. The design methodology computes the optimal

controller output considering constraints of the frequency deviation and load disturbance. The overall dynamic performance of H_∞ + LQG is simulated considering different operation conditions. A comparison among the system with H∞ alone, H∞ + WT, and H∞ + LQG + WT control scheme has been performed and presented in the results shown in this chapter. The simulation results proved the influence of the planned scheme. These results showed the superiority of the control system compared to many controllers of wind turbines [21–29].

The rest sections of this chapter have been ordered as follows: The mathematical model of the system has been presented in Sect. 2. The design of H_∞ has been introduced in Sect. 3. LQG is introduced in Sect. 4. The implementation of the overall control system has been presented in Sect. 5. Simulation results and discussions have been introduced in Sect. 6. The conclusion is introduced in Sect. 7.

2 System Dynamics

A. Mathematical description of a single-area system

The structured frequency response of a single-area power system is presented in Ref. [14]. The overall generator–load dynamic mathematical description is rewritten as shown in the following equations:

$$\boldsymbol{p}.\Delta\mathbf{f} = \left(\frac{1}{2\mathbf{H}}\right)\cdot\Delta\mathbf{P_m} - \left(\frac{1}{2\mathbf{H}}\right)\cdot\Delta\mathbf{P_L} - \left(\frac{\mathbf{D}'}{2\mathbf{H}}\right)\cdot\Delta\mathbf{f} \tag{1}$$

$$p\cdot\Delta\mathrm{P_m} = \left(\frac{1}{\mathrm{T_t}}\right)\cdot\Delta\mathrm{P_g} - \left(\frac{1}{\mathrm{T_t}}\right)\cdot\Delta\mathrm{P_m} \tag{2}$$

$$p\cdot\Delta\mathrm{P_g} = \left(\frac{1}{\mathrm{T_g}}\right)\cdot\Delta\mathrm{P_c} - \left(\frac{1}{\mathrm{R.T_g}}\right)\cdot\Delta\mathrm{f} - \left(\frac{1}{\mathrm{T_g}}\right)\cdot\Delta\mathrm{P_g} \tag{3}$$

The diagram showing the logic used in this controller for the power system has been shown in Fig. 1. Equations (1–3) can be rewritten as a state-space model as shown in the following equations:

$$\begin{bmatrix} p\cdot\Delta\mathrm{P_g} \\ p\cdot\Delta\mathrm{P_m} \\ p\cdot\Delta\mathrm{f} \end{bmatrix} = \begin{bmatrix} -\frac{1}{\mathrm{T_g}} & 0 & -\frac{1}{\mathrm{R.T_g}} \\ \frac{1}{\mathrm{T_t}} & -\frac{1}{\mathrm{T_t}} & 0 \\ 0 & \frac{1}{2\mathrm{H}} & -\frac{\mathrm{D}'}{2\mathrm{H}} \end{bmatrix}\begin{bmatrix} \Delta\mathrm{P_g} \\ \Delta\mathrm{P_m} \\ \Delta\mathrm{f} \end{bmatrix} + \begin{bmatrix} 0 \\ 0 \\ -\frac{1}{2\mathrm{H}} \end{bmatrix}\Delta\mathrm{P_L} + \begin{bmatrix} \frac{1}{\mathrm{T_g}} \\ 0 \\ 0 \end{bmatrix}\Delta\mathrm{P_c} \tag{4}$$

$$y = \begin{bmatrix} 0\ 0\ 1 \end{bmatrix}\begin{bmatrix} \Delta\mathrm{P_g} \\ \Delta\mathrm{P_m} \\ \Delta\mathrm{f} \end{bmatrix} \tag{5}$$

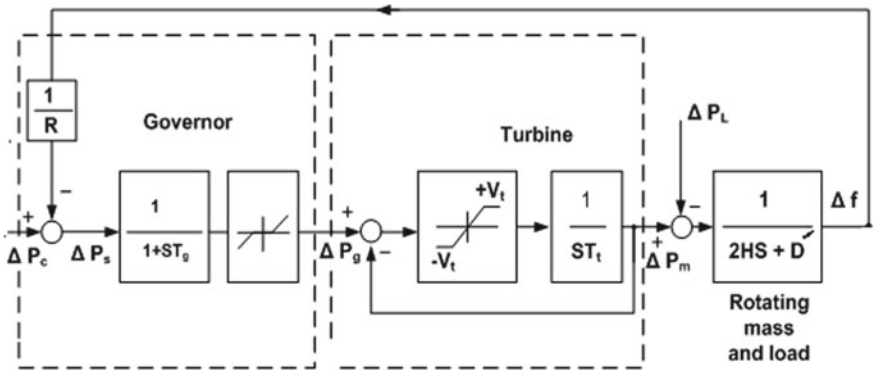

Fig. 1 The uncontrolled single-area power system

where ΔP_g denotes the governor's output variation. ΔP_m denotes the mechanical power variation. Δf denotes the frequency aberration. ΔP_L represents the load change while ΔP_c denotes supplementary control action; and p is a differential operator. While $\left(\frac{1}{s}\right)$ denotes integral Laplace. Furthermore, T_g and T_t represents the governor and turbine time constants. y denotes output. While H denotes an equivalent inertia coefficient. Also, D denotes equivalent damping constant. Moreover, R denotes the speed droop characteristic.

B. Mathematical Model of Wind Turbine based DFIG

Figure 2 displays a model of DFIG WT using the frequency response [14]. The presented model of the frequency response can be written as shown in the following

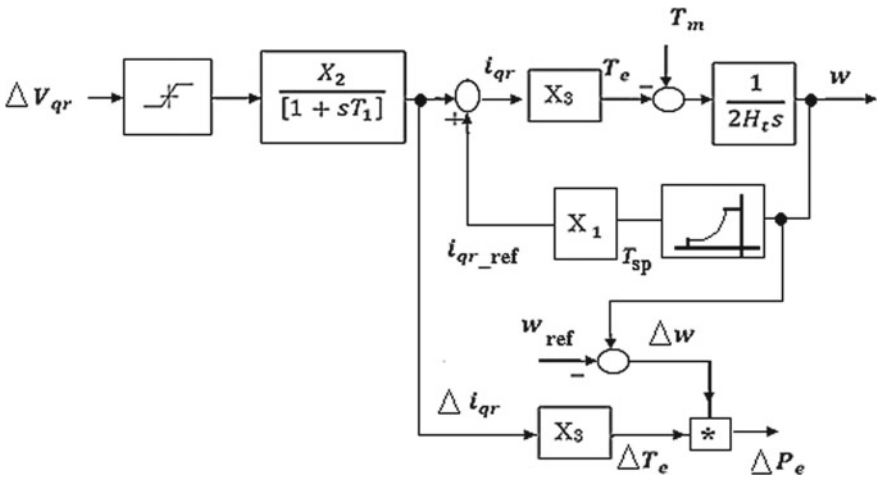

Fig. 2 Model of DFIG WT [14]

Table 1 The parameters shown in of Fig. 2

X_2	X_3	T_1
$\frac{1}{R_s}$	$\frac{L_m}{L_{ss}}$	$\frac{L_0}{\omega_s R_s}$

equations:

$$s \cdot i_{qr} = -\left(\frac{1}{T_1}\right) \cdot i_{qr} + \left(\frac{X_2}{T_1}\right) \cdot V_{qr} \tag{6}$$

$$s \cdot \omega = -\left(\frac{X_3}{2H_t}\right) \cdot i_{qr} + \left(\frac{X_2}{2H_t}\right) \cdot T_m \tag{7}$$

$$P_e = \omega \cdot X_3 \cdot i_{qr} \tag{8}$$

For linearization, Eq. (14) can be represented as shown in the following equation:

$$P_e = \omega_{opt} \cdot X_3 \cdot i_{qr} \tag{9}$$

where ω_{opt} denotes the operating point of the rotational speed. While T_e denotes electromagnetic torque, T_m denotes the mechanical torque, ω denotes the rotational speed. Moreover, P_e denotes the active power of wind turbine, i_{qr} denotes q-axis rotor current, v_{qr} denotes q-axis rotor voltage. H_t denotes equivalent inertia of WT. Table 1 displays the applied parameters with respect to Fig. 2.

where

$L_{ss} = L_s + L_m$,
$L_{rr} = L_r + L_m$,
$L_0 = L_{rr} + \frac{L_m^2}{L_{ss}}$.

ω_s represents synchronous speed, while L_m represents the magnetizing inductance. Moreover, R_r and R_s represent rotor and stator resistances, respectively. Furthermore, L_r and L_s represent rotor and stator leakage inductances. Moreover, L_{rr} and L_{ss} denote rotor and stator self-inductances, respectively.

3 H_∞ Infinity Controller

The producer of the design the H_∞ control scheme mainly depends on the static or dynamic feedback controller. So, H_∞ synthesis has been approved as the following:

i. Formulation: determining the weighting functions of the input and output to accomplish the robustness and performance necessities.
ii. Solution: the weighting functions may be modified to reach the optimal design of the controller.

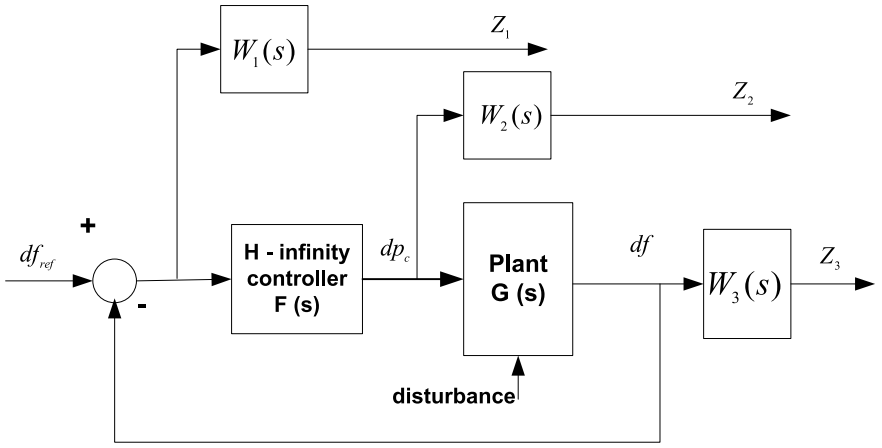

Fig. 3 Scheme of the plant with H_∞

In the proposed wind generation system including H_∞ controller, The system G(s) is the plant with weighting functions of $W_1(s)$ corresponding the signals of error while the $W_2(s)$ corresponding the signals of control and $W_3(s)$ corresponding the signals of output. The proper selecting of the weighting functions is the core of H_∞ scheme.

Considering the control system of Fig. 3. The sets of weighting functions have been chosen to ensure robust performance goals as the following.

The $W_1(s)$ assists to realize a good tracking performance, which means in this case that frequency deviation equals zero. Moreover, the other benefit of the proper choice of this weighting function is the rejecting of the disturbances. This can be expressed mathematically as

$$Z_1 = W_1(s)[0 - \Delta f] \tag{10}$$

The other weight transfer function $W_2(s)$ helps to provide the robustness to plant additive perturbations. This can be expressed mathematically as:

$$Z_2 = W_2(s) \,.\, u(s) \tag{11}$$

where $u(s)$ denotes output control signals for H_∞ regulator.

Finally, the function $W_3(s)$ is essential to determine the closed-loop bandwidth and sensor noise attenuation at high frequencies, mathematically can be described as shown in the following equation:

$$Z_3 = \quad W_3(s) \quad [P] \tag{12}$$

4 Linear Quadratic Gaussian (LQG)

The LFC for a single-area power system has been established using H∞ and LQG techniques in this Chapter. The LQG is planned using the linear model of the plant, an integral objective function, and also Gaussian white noise model of disturbance and noise. Moreover, the LQG involves an optimal state feedback gain "k" and the Kalman estimator. Furthermore, the optimal feedback gain has been estimated to achieve the feedback control law u = −kx resulting in the minimization of the following performance index:

$$H = \int_0^\infty \left(X^T QX + u^T Ru\right)dt \tag{13}$$

where Q and R denote the positive definite or semidefinite Hermitian or real symmetric [15]. Moreover, the optimal state feedback u = −kx could be implemented considering the plant's full state. So, the states have been preferred to be frequency variation Δf, mechanical power change ΔP_{mi}, and governor output change ΔP_g. The Δf and ΔP_c have been measured and have been considered as inputs to the Kalman estimator. The Kalman filter has been utilized in order to observe the following unmeasured states:

$$\hat{x} = \left[\, \Delta\hat{f} \;\; \Delta\hat{p}_m \;\; \Delta\hat{p}_g \,\right]$$

The states observation has been estimated based on the following equation:

$$\left(\dot{\hat{x}}\right) = (A - Bk - LC)\hat{x} + Ly \tag{14}$$

where L denotes the Kalman gain. Moreover, the value of the L can be calculated considering the matrices of Q_n and R_n.

5 System Configuration

The control scheme of the complete system has been illustrated in Fig. 4. The system contains a simplified frequency response model for a single-area power system considering the integration of the wind energy system and including the proposed controller H∞ and LQG estimator has been illustrated in Fig. 4.

The measured and reference frequency deviation Δf and $\Delta f_{ref} = 0$ Hz have been applied as the inputs of H∞ controller to get the supplementary control action ΔP_c. Moreover, the frequency deviation Δf and supplementary control action ΔP_c are used as the input of the Kalman filter for estimating the states of

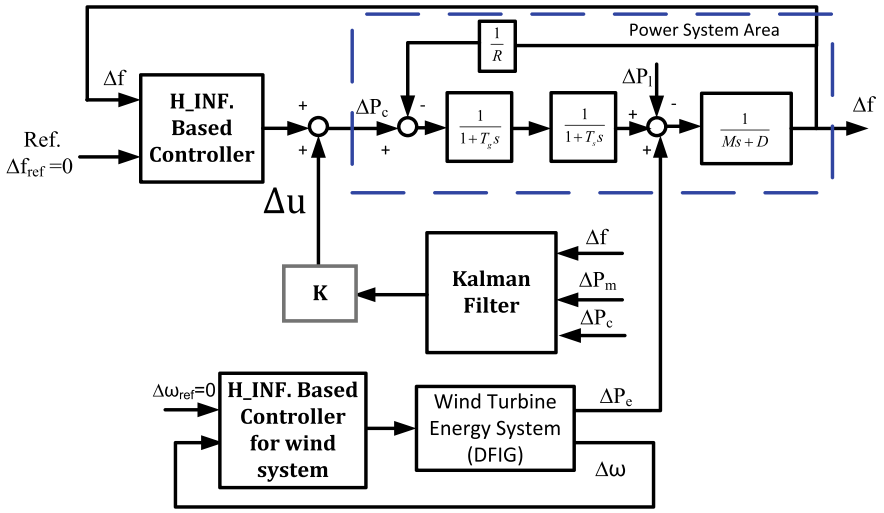

Fig. 4 Single area power system with wind energy system considering the proposed H∞ and LQG controllers

$\hat{x} = \left[\Delta\hat{f}\ \Delta\hat{p}_m\ \Delta\hat{p}_g\right]$. The observed states are growing with the optimal state feedback gain "k" for getting the optimal control signal.

The subsequent set of weighting functions have been selected after many iterations in order to achieve the favorite robustness.

For the power system plant, the weighting functions are

$W_1 = \frac{s+0.3}{s+0.56}$, $W_2 = \frac{s}{s+0.04}$, and $W_3 = \frac{1}{s+2}$.

While for the wind turbine energy system are

$W_1 = 1$, $W_2 = 0$, and $W_3 = \frac{1}{s}$.

Each model of the plant and the Wind turbine DFIG has been modeled in Simulink as input–output system. Then, the MATLAB tool of *linmod* has been used to extract a continuous-time linear state-space model. This model is used to plan the robust controllers of H_∞ and LQG.

6 Results and Discussions

Simulation tests are executed to confirm the effectiveness of the presented control system considering H∞ and LQG controllers in MATLAB/Simulink platform. All parameters of the system are detailed in Table 2 [2]. Moreover, the data of the DFIG WT are detailed in Table 3.

The WT involves 200 of 2 MW of VSWTs. Moreover, the parameters of WT have been specified in Table 3.

X_m denotes magnetizing reactance. Also, X_{ls} and X_{lr} denote leakage reactance of the rotor and stator, respectively.

Table 2 Single area power system parameters

D (pu/Hz)	$2H$ (pu.sec)	R (Hz/pu)	T_g (s)	T_t (s)
0.015	0.1667	3.00	0.08	0.40

$(p_e)_{\text{Base}} = 800$ MVA

Table 3 The WT parameters [14]

Operating point (MW)	Wind speed (m/s)	Rotational speed
247	11	1.17
R_r (pu)	R_s (pu)	X_{lr} (pu)
0.00552	0.00491	0.1
X_{lr} (pu)	X_m (pu)	H_t (pu)
0.09273	3.9654	4.5

The generation rate constraint (GRC) of 10% per minute is considered. Moreover, the maximum value of the dead band for governor has been considered as 0.05 pu [2].

Case study 1

In this case of study, wind turbine participation is simulated at nominal parameters and specifications. Two tests have been carried out, the first is to test the system performance with WT. While the second test has been considering the absence of the WT. The two cases of tests have been compared with respect to the frequency deviation and the variation of mechanical power. A step load change is applied with the value of 0.02 pu at the time of $t = 50$ s. Figure 5 shows the simulation results of this case study. In this case, the parameter and data of the power plant are assumed as the nominal data. So, it is clear the performance of both two cases is stable. However, it is exposed to the results that the system is slow compared to those without the participation of WT because of the absence of the WT inertia. The assumed variation of the wind turbine speed has also been illustrated in the figure.

Case study 2

To validate the proposed $\mathbf{H}_\infty$ + LQG controller with wind turbine participation, the dynamic performance of the control system has been simulated at nominal parameters under step load change of 0.06 pu. The simulation results of this case under study have been revealed in Fig. 6. This figure displays that the performance of the proposed controller system with wind turbine participation is better than those without wind turbine participation. The overshoot is decreasing from 0.05626 to 0.0205 with wind turbine participation. So, integration of the WT led to the enhancement of the features of the planned controller of $\mathbf{H}_\infty$ + LQG in this case of study.

Case study 3

The system parameters are varied in this case of study for authenticating the robustness of controller performance. The system is tested under parameter uncertainty

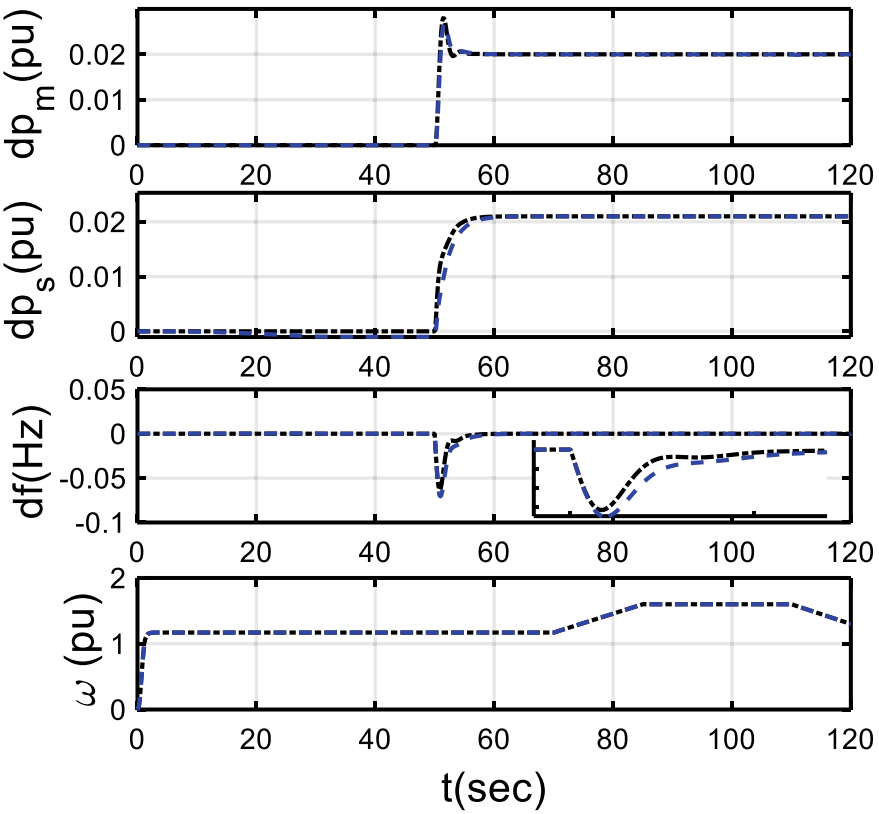

Fig. 5 Control system response for case 1; with $\mathbf{H}_\infty$ + LQG controller with the participation of wind turbines (dash blue curve), $\mathbf{H}_\infty$ + LQG controller without the participation of wind turbines (dash-dot black curve)

of the damping and inertia. The simulation results have been shown in Fig. 7. The system performance under parameter uncertainty is still stable and the proposed controller with the wind turbine participation is capable of damping the oscillations. Moreover, the features of the designed H_∞ + LQR is associated with those of the H_∞ controller only. The comparison shows that the proposed controller of H_∞ + LQR has the best performance considering overshoot.

Case study 4

In this case of study, the performance of the system has been investigated considering connecting the WT and disconnecting the WT at 40 and 100 s, respectively. The load will be assumed o be 0.01 pu at 5 s and is not changed to the end of the simulation time. The results of this case under study have been exposed in Fig. 8. The figure displays the performance of the H_∞ + LQG and conventional I controllers for the purpose of comparison and validation. The figure illustrates ΔP_m, ΔP_s, Δf, and ω from top to bottom. From the figure, the performance of the H_∞ + LQG is the best

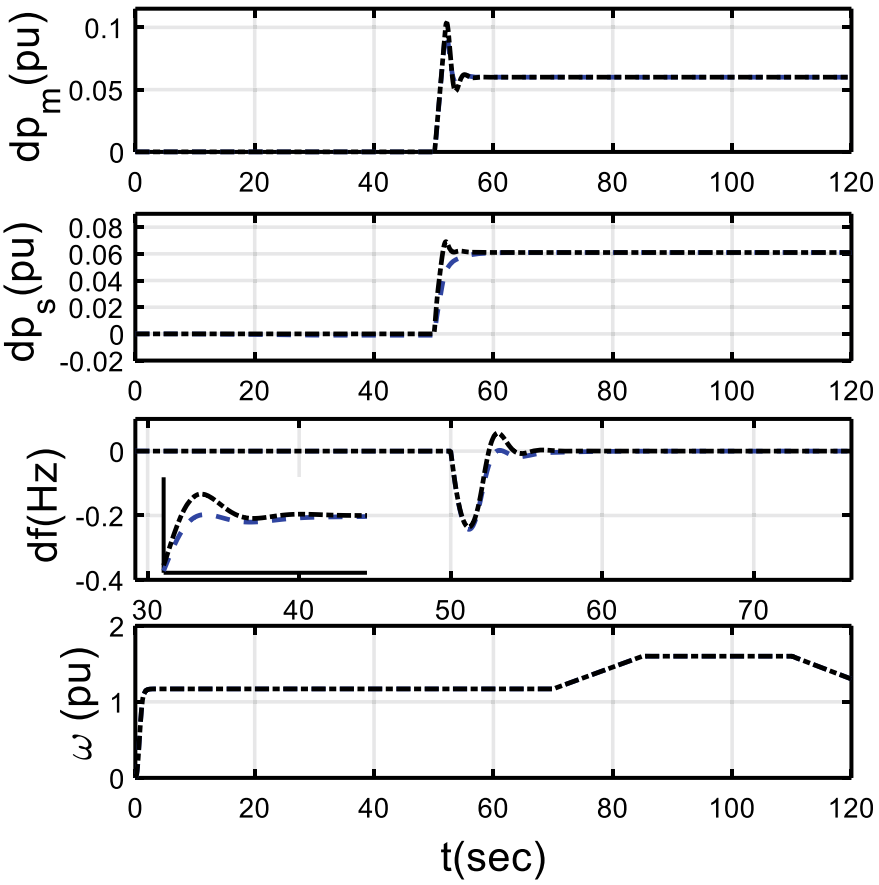

Fig. 6 Control system response for case 2; with **H_∞+ LQG** controller with participation of wind turbines (dash blue curve), **H_∞+ LQG** controller without participation of wind turbines (dash-dot black curve)

one concerning the fast response and lower overshooting. While the H_∞ + LQG controller has a very high performance, the conventional I controller performance is the lowest one.

7 Conclusion

In this chapter, an LFC control scheme considering the H_∞ and LQG is planned for a single-area power system bearing in mind the wind turbine energy system. The future controllers are planned to work in parallel to guarantee overall stability. Moreover, the simulation tests have been applied to validate the control system under different

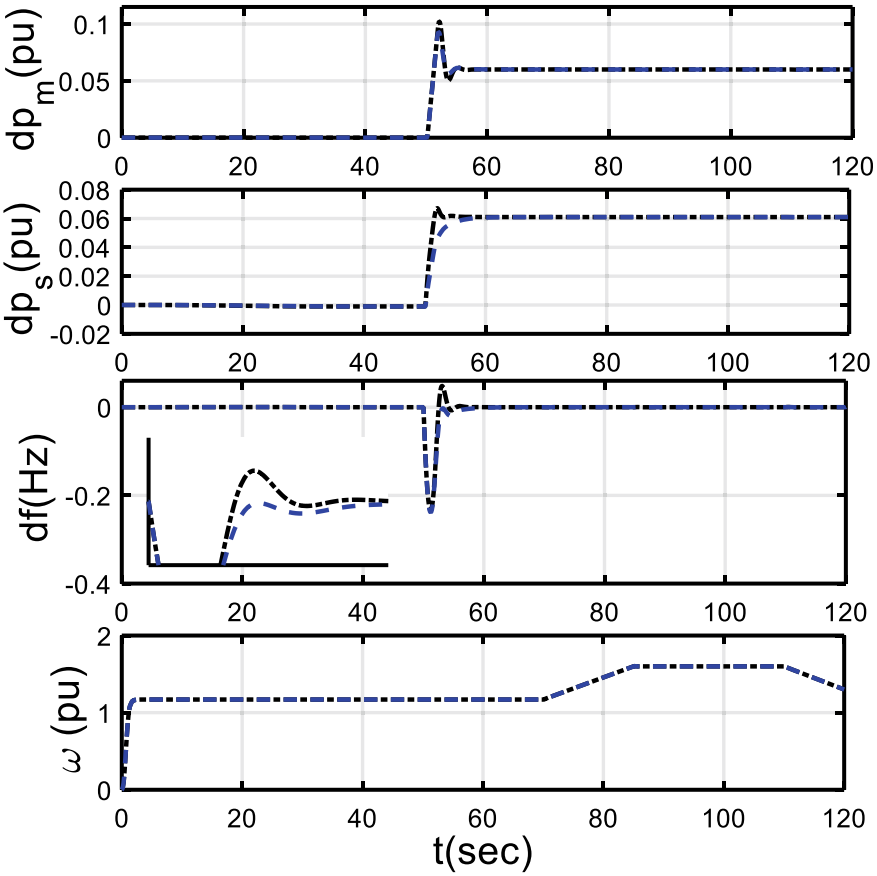

Fig. 7 Control system response for case 3; with $\mathbf{H_\infty}$ **+ LQG** controller with the participation of wind turbines (dash blue curve), $\mathbf{H_\infty}$ controller with the participation of wind turbines (dash-dot black curve)

load changes and parameter uncertainties. The overall performance of the proposed controller of H_∞ + LQG has been compared with those of H_∞ and conventional I controller. The obtained results confirmed that the planned H_∞ + LQG has acceptable performance and stability. Furthermore, the designed H_∞ + LQG has been proven as a robust controller in contrast to the load variation and parameter uncertainties. Also, the results specified that the combination H_∞ + LQG and H_∞ controllers can give the required robustness. However, the H_∞ + LQG can give a better dynamic response especially in the case of considering the wind turbine energy system. Moreover, the priority and effectivity of the H_∞ + LQG controller are validated in the case of severing parameter uncertainties more than H_∞ controller.

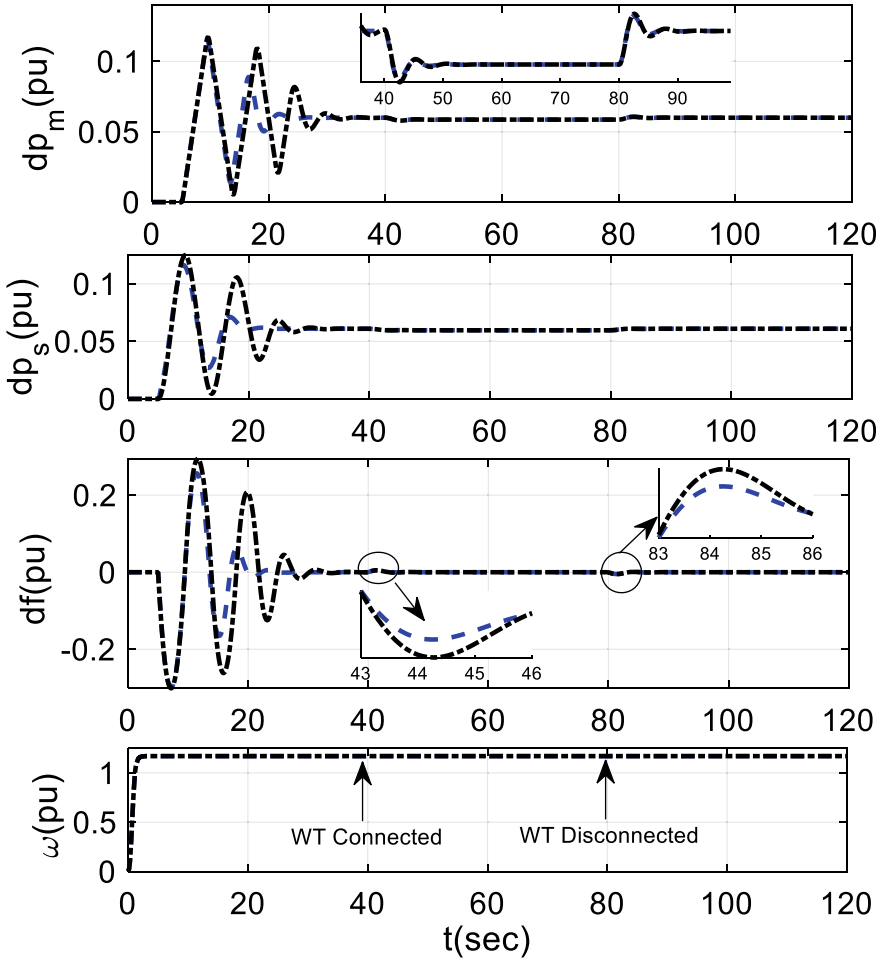

Fig. 8 Control system response for case 4; with $\mathbf{H_\infty}$ **+ LQG** controller (dash blue curve), Conventional **I** controller (dash-dot black curve)

References

1. Kundur P (1994) Power system stability and control. McGraw-Hill, New York
2. Bevrani H (2009) Robust power system control. Springer, New York
3. Eltamaly AM, Mamdooh A-S, Sayed K, Abo-Khalil AG (2020) Sensorless active and reactive control for DFIG wind turbines using opposition-based learning technique. Sustainability 12(9):3583
4. Mohamed, TH, Zaki Diab AA, Hussein MM (2015) Application of linear quadratic gaussian and coefficient diagram techniques to distributed load frequency control of power systems. Appl Sci 5(4):1603–1615
5. https://www.irena.org/. Accessed 18 March 2020

6. Holdsworth L, Ekanayake JB, Jenkins N (2004) Power system frequency response from fixed speed and doubly fed induction generator-based wind turbines. Wind Energy 7:21–35
7. Eltamaly AM, Al-Saud MS, Abo-Khalil AG (2020) Dynamic control of a DFIG wind power generation system to mitigate unbalanced grid voltage. IEEE Access 8:39091–39103
8. Abo-Khalil AG, Alghamdi AS, Eltamaly AM, Al-Saud MS, RP P, Sayed K, Bindu GR, Tlili I (2019) Design of state feedback current controller for fast synchronization of DFIG in wind power generation systems. Energies 12:2427
9. Mohamed, MA, Zaki Diab AA, Rezk H (2019) A novel adaptive model predictive controller for load frequency control of power systems integrated with DFIG wind turbines. Neural Comput Appl 1–11
10. Mullane A, O'Malley M (2005) The inertial response of induction-machine-based wind turbines. IEEE Trans Power Syst 20(3):1496–1503
11. Lee HJ, Park JB, HoonJoo (2006) Robust LFC for uncertain nonlinear power systems: a fuzzy logic approach. Inf Sci 176:3520–3537
12. Rerkpreedapong D, Hasanovic A, Feliachi A (2003) Robust load frequency control using genetic algorithms and linear matrix inequalities. IEEE Trans Power Syst 18(2):855–861
13. Demiroren A, Zeynelgil HL, Semgor NS (2001) The application of ann technique to load-frequency control for three-area power system. In: Paper accepted for presentation at PPT 2001, 2001 IEEE porto power tech conference 10th–13th September, Porto, Portugal
14. Liu F, Song YH, Ma J, Mai S, Lu Q (2003) Optimal load-frequency control in restructured power systems. IEE Proc Gener Trans Distrib 150(1):87–95
15. Wang Y, Hill DJ, Guo G (1998) Robust decentralized control for multimachine power system. IEEE Trans Circuits Syst Fundam Theory Appl 45(3)
16. Stankovic AM, Tadmor G, Sakharuk TA (1998) On robust control analysis and design for load frequency regulation. IEEE Trans Power Syst 13(2):449–455
17. Pan CT, Liaw CM (1989) An adaptive controller for power system load-frequency control. IEEE Trans Power Syst 4(1):122–128
18. Cam E, Kocaarslan I (2005) Load frequency control in two area power systems using fuzzy logic controller. Energy Convers Manag 46:233–243
19. Birch AP, Sapeluk AT, Ozveren CS (2005) An enhanced neural network load frequency control technique. Control 94:21–24, Conference Publication No. 389, IEE 1994. ASCE J 5(II)
20. Abdel-Magid YL, Dawoud MM (1995) Genetic algorithms applications in load frequency control. In: Genetic algorithms in engineering systems: innovations and applications, 12–14 September 1995, conference publications No. 414, IEE
21. Diab AAZ, Al-Sayed A-HM, Mohammed HHA, Mohammed YS (2020) Development of adaptive speed observers for induction machine system stabilization. Springer
22. Abo-Khalil AG, Alghamdi A, Tlili I, Eltamaly AM (2019) Current controller design for DFIG-based wind turbines using state feedback control. IET Renew Power Gener 13(11):1938–1948
23. Eltamaly AM, Mohamed YS, El-Sayed A-HM, Elghaffar ANA (2019) Analyzing of wind distributed generation configuration in active distribution network. In: 2019 8th international conference on modeling simulation and applied optimization (ICMSAO), pp 1–5 (2019)
24. Eltamaly AM, Mohamed YS, El-Sayed A-HM, Elghaffar ANA (2019) Reliability/security of distribution system network under supporting by distributed generation. Insight-Energy Sci 2(1):1–14
25. Eltamaly AM, Farh HM (2013) Maximum power extraction from wind energy system based on fuzzy logic control. Electr Power Syst Res 97:144–150
26. Eltamaly AM, Alolah AI Abdel-Rahman MH (2011) Improved simulation strategy for DFIG in wind energy applications. Int Rev Model Simul 4(2)
27. Eltamaly AM (2007) Modeling of wind turbine driving permanent magnet generator with maximum power point tracking system. J King Saud Univ-Eng Sci 19(2):223–236
28. Eltamaly AM, Alolah AI, Abdel-Rahman MH (2010) Modified DFIG control strategy for wind energy applications. In: SPEEDAM, pp 653–658. IEEE
29. Eltamaly AM, Alolah AI, Farh HM, Arman H (2013) Maximum power extraction from utility-interfaced wind turbines. New Dev Renew Energy 159–192